Journal of Fluorescence, Vol. 1, No. 1, 1991

Rotamer-Specific Fluorescence Quenching in Tyrosinamide: Dynamic and Static Interactions

Paul Brian Contino[1] and William R. Laws[1,2]

Received October 8, 1990; accepted December 4, 1990

We have examined the environments of the three phenol rotamers about the C^{α}–C^{β} bond in tyrosinamide by fluorescence quenching. Steady-state acrylamide quenching yields a nonlinear Stern–Volmer plot. With three distinct emitting species and no other information about the system, it is impossible to analyze the data due to the number of variables which have to be determined. We therefore reduced the number of variables by independently determining the fractional intensity and dynamic quenching constant for each rotamer through time-resolved fluorescence quenching studies. These parameters were then used to analyze the steady-state data for any contribution of static quenching. We conclude that the nonlinear Stern–Volmer plot for the quenching of tyrosinamide by acrylamide is a consequence of each rotamer having a distinct dynamic quenching constant and the presence of static quenching. The static quenching can be represented by either the sphere-of-action model involving two of the three rotamers or the ground-state complex model involving all three rotamers.

KEY WORDS: Fluorescence; tyrosine; rotamers; dynamic and static quenching.

INTRODUCTION

The addition of a quenching agent is a common technique to characterize the environment of a fluorescent chromophore in a biological system. If the chromophore is in several different environments, resulting in ground-state and therefore excited-state heterogeneity, then several chromophore classes are present. Consequently, the fluorescence intensity decay kinetics of the system could be complex and described by a sum of exponentials [1,2] or a distribution of rates [3]. When this occurs, the Stern–Volmer expression [4] used to analyze steady-state fluorescence quenching data from a single chromophore must be modified to account for multiple species [5]. Other processes can also affect the Stern–Volmer expression, including (i) excited-state reactions resulting in complex intensity decay kinetics and (ii) static quenching resulting in inconsistencies between steady-state and time-resolved data.

In previous studies, we examined the fluorescence intensity decay kinetics of tyrosine, tyrosine model compounds, and the tyrosine residue in the peptide hormone oxytocin [6,7]. We found that in each case the fluorescence intensity decay kinetics were complex and required a sum of exponentials to fit the lifetime data. We were able to correlate the preexponential amplitude terms, which can reflect the initial excited-state populations for each kinetic species, with the ^{1}H-NMR-determined ground-state rotamer populations for the tyrosine side chain about the C^{α}–C^{β} bond. This correlation between the fluorescence decay kinetics and the ^{1}H-NMR results suggested that the complex decay kinetics were due to multiple ground-state tyrosine species (rotamers) that do not interconvert during the lifetimes of the excited states [6,7]. There was no evidence for an excited-state reaction.

[1] Department of Biochemistry, Mount Sinai School of Medicine, New York, New York 10029.

[2] To whom correspondence should be addressed at Department of Biochemistry, Mount Sinai School of Medicine, One Gustave L. Levy Place, New York, New York 10029.

1053-0509/91/0300-0005$06.50/0

The existence of excited-state rotamers having unique lifetimes implies that each rotamer has a distinct environment with different kinetic constants for nonradiative processes. Thus, heterogeneity due to different molecular orientations can occur even in a chemically pure system. To examine the differences in the environments of the three rotamers, we have performed fluorescence quenching studies on tyrosinamide. The initial analysis of the nonlinear, steady-state Stern–Volmer plot by a multiple ground-state species model did not provide a unique solution. Simulation studies mirrored this difficulty and demonstrated the need to reduce the number of variables. (The Stern–Volmer constant and fractional intensity must be determined for each rotamer.) If static quenching processes are also involved, then additional variables have to be evaluated.

We have analyzed these data by taking a systematic, three-step approach. First, the amplitude and lifetime for each rotamer were determined as a function of the acrylamide concentration. This was facilitated by linking the amplitudes during the analysis of the time-resolved data to the rotamer populations that had been independently determined by ^{1}H-NMR [6]. This reduced the number of intensity decay parameters that had to be determined from six (three lifetimes and three amplitudes) to four (three lifetimes and one amplitude) and allowed the lifetimes to be determined with greater precision [6–8]. The amplitudes and lifetimes in the absence of acrylamide were then used to calculate the fractional intensities of each rotamer. Second, the lifetimes as a function of acrylamide concentration were used to obtain the rotamer-specific Stern–Volmer constants, which were in turn used to calculate the individual dynamic bimolecular quenching constants. In this way, all the dynamic quenching parameters for each rotamer were independently determined by time-resolved fluorescence quenching studies. Third, these dynamic quenching parameters were used to evaluate the steady-state quenching data; we found that static quenching was also present. Because we reduced the number of quenching parameters, the steady-state data could be analzyed further for static quenching parameters. We compared two static quenching mechanisms; both provided physically relevant parameters and acceptable fits and neither one could be eliminated.

MATERIALS AND METHODS

Chemicals. L-Tyrosinamide (TyrA) was obtained from Vega Biotechnologies, Inc., and was checked for purity by thin-layer chromatography and by comparison to the absorbance and fluorescence spectra of L-tyrosine. All other chemicals were reagent grade. All solutions were prepared in deionized H_2O at pH 3.0 (HCl).

Steady-State Fluorescence Quenching. Steady-state fluorescence quenching data and uncorrected spectra were obtained using an SLM 4800 fluorometer modified by us for single-photon counting and interfaced to a personal computer. Steady-state fluorescence quenching data were collected at 5.0 ± 0.5°C in a 1.0 × 0.4-cm-pathlength quartz cuvette by the cumulative addition of small volumes of a concentrated acrylamide solution. Samples were excited (1-cm pathlength) at 285 nm (4-nm bandpass) and the fluorescence emission was monitored at 305 nm (8-nm bandpass) using excitation and emission polarizers oriented to obtain an emission intensity proportional to the total fluorescence intensity [9–12]. The optical density of the samples prior to quenching was between 0.10 and 0.20 at 285 nm. Each quenched fluorescence intensity value, F, was referenced to the intensity of an unquenched sample, F_0, to account for any instrumental fluctuation or time-dependent sample deterioration.

Each F and F_0 was an average of five 10-s integrations and was corrected for phototube dark counts and solvent blank. Each F was also corrected for dilution and inner filter effects to give a corrected quenched intensity, F_c:

$$F_c = F\left(\frac{V_t}{V_o}\right)\left\{\text{antilog}\left[\frac{\epsilon_{ex}(V_t - V_o)[Q_s]}{2V_t} + \frac{\epsilon_{em}(V_t - V_o)[Q_s]}{2V_t}\right]\right\}$$

where V_o is the initial volume, V_t is the total volume after each addition of quencher, ϵ_{ex} and ϵ_{em} are the extinction coefficients of the quencher at the excitation and emission wavelengths, respectively, and $[Q_s]$ is the concentration of the stock quencher solution. In this expression, the volume ratio is the dilution correction and the antilog term contains the primary and secondary inner filter corrections due to absorption of light by the quencher, taking into account the geometry of the optics [13].

Time-Resolved Fluorescence Quenching. Time-resolved fluorescence quenching data were collected at 5.0 ± 0.5°C. Samples were excited at 285 nm and the fluorescence was monitored at 305 nm (5-nm bandpass) in a time-correlated single-photon counting fluorometer [14]. Decay curves were collected into 4000 channels at 11 ps/channel. The instrument response function was 225 ps wide at full-width at half-maximum. The fluorescence

intensity decay curves, $I(t)$, were analyzed by nonlinear least-squares regression [15] using a sum of exponentials [1,2]:

$$I(t) = \sum_{i=1}^{n} \alpha(i)\, e^{-t/\tau(i)}$$

where $\alpha(i)$ is the amplitude and $\tau(i)$ is the lifetime for each of n components. Each $I(t)$ was also analyzed by scaling the $\alpha(i)$ terms to the ^{1}H-NMR-determined rotamer populations using the linked-function method [6–8].

THEORY

The fluorescence lifetime, τ_o, of a simple chromophore in a noninteracting system is given by $(k_{nr} + k_f)^{-1}$, where k_{nr} is the sum of all the rate constants for nonradiative decay processes and k_f is the rate constant for fluorescence. The addition of a collisional quenching agent decreases the observed lifetime, τ, due to the addition of another term to this expression: $(k_{nr} + k_f + k_q[Q])^{-1}$, where k_q is the bimolecular quenching constant and $[Q]$ is the quencher concentration. In the absence of static quenching, the steady-state fluorescence intensities, F_o and F, are directly comparable to the two respective lifetimes. Assuming that there is no effect on the extinction of the chromophore by the quenching agent, a ratio can be expressed:

$$F_o/F = \tau_o/\tau = (k_{nr} + k_f)^{-1}/(k_{nr} + k_f + k_q[Q])^{-1} \quad (1)$$

By rearranging and defining $K_{sv} = k_q/(k_f + k_{nr})$, Eq. (2) is obtained, which is the classic, linear Stern–Volmer relationship [4]:

$$F_o/F = \tau_o/\tau = 1 + K_{sv}[Q] \quad (2)$$

Static quenching and/or multiple species can cause nonlinear steady-state fluorescence Stern–Volmer plots [5,16]. Static quenching is implicated when the quantum yield measured by steady-state methods is less than that measured by time-resolved methods. Static quenching can be viewed as an extremely rapid process that effectively deactivates a fraction of the excited-state population before it can be dynamically quenched.

Two static quenching mechanisms are commonly considered. In the sphere-of-action model, there is a finite probability that a quencher molecule is already within a volume element V that is sufficiently close to the chromophore upon excitation that quenching occurs "instantaneously" without a diffusion-controlled collisional interaction [5]. Since the distribution of quencher molecules is random, the probability of this static quenching process is described by a Poisson distribution as expressed in Eq. (3):

$$F_o/F = (1 + K_{sv}[Q])\, e^{V[Q]} \quad (3)$$

In the ground-state complex model, the quencher and chromophore may form a weak, 1:1 complex with an association constant K_a. This complex reaches its initial Franck–Condon state but is efficiently quenched, again due to the fact that diffusion does not occur. The correction for this type of static quenching arises from the equilibrium expression for the complex, and Eq. (4) results [5]:

$$F_o/F = (1 + K_{sv}[Q])(1 + K_a[Q]) \quad (4)$$

The presence of several chromophores with distinct lifetimes, and therefore with distinct K_{sv} terms, can also cause deviations from the linearity of Eq. (2). These multiple species could arise from more than one type of chromophore, a chemically pure chromophore associated at different sites of a biological molecule, or a chemically pure chromophore residing at a single site that has different structural conformations producing different local environments. Assuming that the different species do not interact, their fluorescence intensities, $f(i)$, are additive. In the case of collisional quenching alone, the modification of the Stern–Volmer expression for n species is Eq. (5):

$$F_o/F = \left[\sum_{i=1}^{n} \frac{f(i)}{(1 + K_{sv}(i)[Q])}\right]^{-1} \quad (5)$$

Depending on the $f(i)$ and $K_{sv}(i)$ values, the F_o/F expression may be linear or curved downward [5].

Each species could also be statically quenched [16]. Equation (6) represents the addition of the sphere-of-action concept to the multiple-species model:

$$F_o/F = \left[\sum_{i=1}^{n} \frac{f(i)}{(1 + K_{sv}(i)[Q])\, e^{V(i)[Q]}}\right]^{-1} \quad (6)$$

The possibility of each species being in a ground-state, 1:1 complex with the quencher is expressed in Eq. (7):

$$F_o/F = \left[\sum_{i=1}^{n} \frac{f(i)}{(1 + K_{sv}(i)[Q])(1 + K_a(i)[Q])}\right]^{-1} \quad (7)$$

For both static quenching mechanisms given by Eqs. (6) and (7), the trend in the F_o/F data will be complex depending on the values of the parameters. If static quenching is occurring, it can mask the downward curvature

effect of different K_{sv} terms and actually cause upward curvature.

RESULTS

Six steady-state fluorescence quenching titrations of TyrA by acrylamide are presented in Fig. 1. At low acrylamide concentrations (0.1 to 0.2 *M* range typically used in fluorescence quenching studies), the data could be viewed as linear. It is only at the higher concentrations that upward curvature of F_o/F_c is observed. Since the fluorescence intensity decay is a sum of three exponentials that can be attributed to multiple species (rotamers) [6], we attempted to analyze the data by Eq. (5). Using the standard Marquardt nonlinear least-squares approach [15], a unique solution could not be found. Simulation studies demonstrated that even in ideal circumstances (noiseless data), it is difficult to recover any two of the fractional intensity or Stern–Volmer constant quenching parameters. Since five quenching parameters would have to be determined to analyze these TyrA data by Eq. (5) (three K_{sv} terms and two of the three fractional intensities), the number of unknowns has to be reduced.

From our previous time-resolved fluorescence data [6], we can calculate the fractional intensities of the rotamers in TyrA by the following expression:

$$f(i) = \alpha(i)\,\tau_o(i) \Big/ \sum_{i=1}^{3} \alpha(i)\,\tau_o(i) \qquad (8)$$

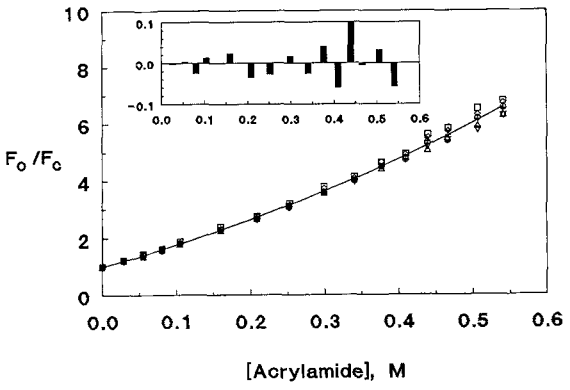

Fig. 1. A Stern–Volmer plot for the steady-state fluorescence quenching of TyrA by acrylamide; see Eq. (2). Six titrations are represented by the different symbols. The line is the best fit, based on averaged parameters, to Eq. (3) (see Discussion). The inset gives the residuals (data—fit) based on the averages of the data points (see Figs. 4 and 5).

The $f(i)$ were then made constants in Eq. (5), reducing the number of unknowns to the three Stern–Volmer constants. However, there were still problems in finding a unique solution.

To allow a complete characterization of the steady-state quenching results in terms of a multiple-species model, we reasoned that the $K_{sv}(i)$ terms as well as the $f(i)$ terms must be known. Equation (9) demonstrates how Eq. (2) can be extended to multiple species:

$$\tau_o(i) / \tau(i) = 1 + K_{sv}(i)[Q] \qquad (9)$$

If each species has a unique, resolvable lifetime and if the species do not interact, then the $K_{sv}(i)$ terms can also be obtained by time-resolved fluorescence.

As we have previously shown [6], the fluorescence intensity decay of TyrA in the absence of quencher can be fit by the sum of two exponentials. The decay can also be equally well analyzed for three exponentials using the linked-function method [8] to scale the $\alpha(i)$ to the rotamer populations [6].

In the experiments described here, three exponentials were always required to fit the intensity decay of tyrosinamide in the presence of acrylamide and the linked-function method did not have to be used. In the analyses for six intensity decay parameters (three τ's and three α's) with no restrictions on any parameters, there were 10–20% variations in the values obtained from repeated titrations. Each lifetime decreased with increasing acrylamide concentration. In contrast, the three amplitude terms did not vary and their values were within 10% of the rotamer populations previously determined by ^{1}H-NMR [6]. The intensity decay data were reanalyzed by linking the rotamer populations to the amplitudes during the regression, and equivalent fits were obtained. In this way, the random variability in the lifetimes was considerably reduced since only four intensity decay parameters (three τ's and one α) instead of six were being iterated [8]. Although several possible associations between rotamer populations and specific lifetimes can be made, only one of these associations was found to work [6,7].

As can be seen in Fig. 2, each rotamer-specific lifetime ratio is linear with respect to acrylamide concentration [Eq. (9)]. The slopes of these lines, which are the $K_{sv}(i)$ terms, were evaluated by linear least squares and are presented in Table I. Since K_{sv} is the product of the bimolecular quenching constant, k_q, and the lifetime in the absence of quencher, τ_o, a k_q value was calculated for each rotamer (Table I). There is a factor of two between the k_q value for rotamer I and that for rotamer III (see Fig. 3 for a description of the rotamers).

We used the quenching parameters determined by

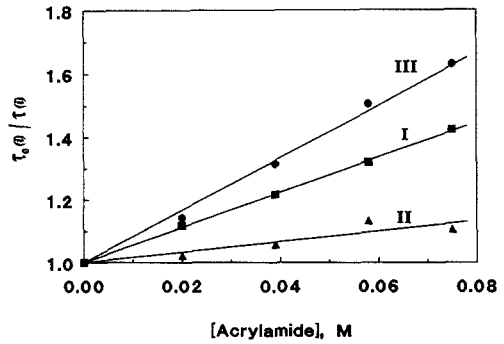

Fig. 2. The Stern–Volmer expressions for each rotamer-associated lifetime: ■, rotamer I; ▲, rotamer II; ●, rotamer III. The lines represent the linear least-squares regression for each lifetime ratio [Eq. (9)].

Table I. Time-Resolved Fluorescence Quenching Parameters[a]

Rotamer	f^b	K_{sv} $(M^{-1})^c$	τ_o (ns)[d]	$k_q \times 10^{-9}$ $(M^{-1}\ s^{-1})^e$
I	0.71	5.59	1.91	2.9
II	0.10	1.66	0.33	5.0
III	0.19	8.36	1.36	6.1

[a]5.0 ± 0.5°C; pH 3.0; 285-nm excitation; 305-nm emission (10-nm bandpass).
[b]The fractional intensity of each kinetic component [Eq. (8)].
[c]Values are the slopes of the regressions shown in Fig. 2.
[d]The lifetime of each rotamer in the absence of quencher.
[e]Calculated from $K_{sv} = k_q\tau_o$.

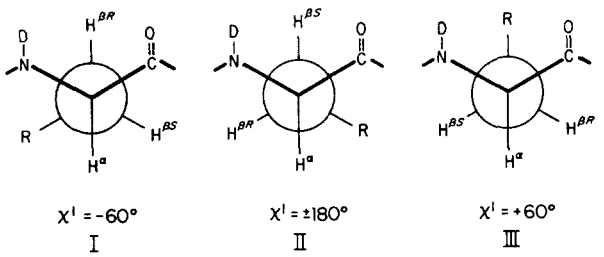

Fig. 3. Newman projections about the C^{α}–C^{β} bond for the possible positions of the phenol group in relation to the C^{α} substituents. The rotamer assignments I, II, and III, and the corresponding values of the torsion angle, χ^1, are indicated for the L configuration of tyrosine. The atom D indicates the protonation state in D_2O, the solvent for the ^{1}H-NMR determination of ground-state rotamer populations.

the time-resolved fluorescence experiments (Table I) to calculate a fit by Eq. (5) to the TyrA steady-state acrylamide quenching data. As shown by the dashed line in Fig. 4, application of the dynamic quenching parameters alone does not follow the steady-state data. To test for static quenching, we tried Eq. (6) with the *V(i)* terms equal to 10% of the individual $K_{sv}(i)$ terms. These initial values were used because *V* terms which are about 10% of K_{sv} have been seen for the acrylamide quenching of indole compounds [5] and a fluorescent steroid [17]. This fit is represented by the dotted-dashed line in Fig. 4; while better, it is not sufficient. For the best fit, *V(i)* had to be near 21% of $K_{sv}(i)$ (not shown). However, the residuals still showed systematic deviations. If we used the $K_{sv}(i)$ and *f(i)* values from Table I in Eq. (6) and then iterated to determine rotamer-specific *V(i)* values, the algorithm tended to force one of the *V* terms to zero. To simplify the analysis, we made that *V* term a constant of zero and reanalyzed. The parameters obtained were used to generate the solid line through the data in Fig. 4; the inset demonstrates acceptable residuals. The *V(i)* values found for rotamers I, II, and III were 1.2, 0, and 2.6 M^{-1}, respectively. Note that these values are within the typical range of 1–3 M^{-1} [5].

Finally, we analyzed the steady-state data by Eq. (7). Our approach was to assume that each rotamer had equivalent K_a values [$K_a(1) = K_a(2) = K_a(3)$]. As shown in Fig. 5, this model provides a fit equivalent to that obtained by the sphere-of-action model above (Fig. 4). The value determined for the common association constant was 1.3 M^{-1}, typical of a weak association.

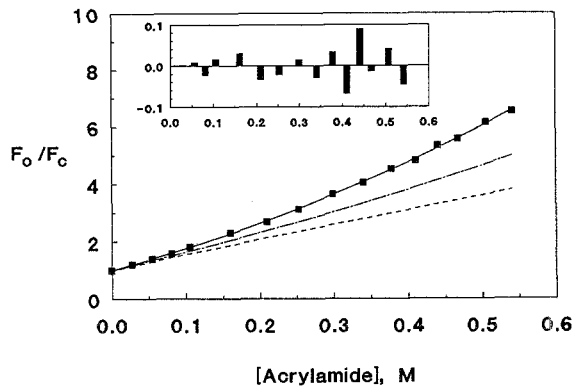

Fig. 4. An evaluation of the steady-state data for TyrA quenched by acrylamide; the data points (■) are the averages of the data in Fig. 1. With *f(i)* and $K_{sv}(i)$ values determined by time-resolved fluorescence quenching measurements (Table I): – – –, the fit generated by Eq. (5); —•—, the fit generated by Eq. (6) with $V(i) = 0.1\ K_{sv}(i)$; ——, the fit generated by Eq. (6) with each *V(i)* term determined by nonlinear least-squares regression (see Results). The inset gives the residuals (data—fit) for the latter fit.

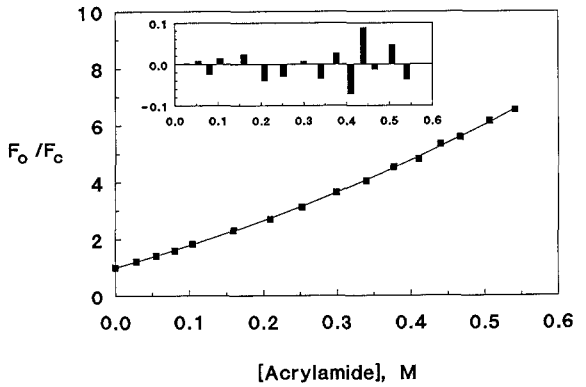

Fig. 5. An evaluation of the steady-state data for TyrA quenched by acrylamide; the data points (■) are the averages of the data in Fig. 1. With $f(i)$ and $K_{sv}(i)$ values determined by time-resolved fluorescence quenching measurements (Table I): ———, the fit generated by Eq. (7) with equal $K_a(i)$ terms determined by nonlinear least-squares regression (see Results). The inset gives the residuals (data—fit) for this fit.

DISCUSSION

Dynamic collisional quenching of a single chromophore yields a linear Stern–Volmer plot [Eq. (2)]. Other processes have been shown to cause deviations from linearity [5]. The nonlinear Stern–Volmer plot in Fig. 1 therefore suggests that other processes must be evaluated for their contribution(s) to the quenching of TyrA by acrylamide. Possible processes include excited-state reactions, static quenching interactions, and multiple species with static quenching. Tyrosine has the potential to undergo excited-state proton transfer [18,19], and the resulting decay kinetics could cause the nonlinear steady-state behavior seen in Fig. 1. Our previous studies on the fluorescence intensity decay of tyrosine, tyrosine analogues, and tyrosine in a small peptide hormone, however, showed no evidence for the formation of excited-state tyrosinate through excited-state proton transfer [6,7]. This absence of the excited-state reaction agrees with the earlier findings of Szabo and co-workers [20]. Furthermore, recent studies have demonstrated that the only way the emission from the excited state of tyrosinate can be observed is through the direct excitation of the ground-state ionic species [21]. Based on these facts, we are excluding an excited-state reaction as the cause of the curvature in Fig. 1.

The presence of multiple species with different K_{sv} terms can result in a steady-state Stern–Volmer plot with downward curvature or may even appear linear [5,16]. We know from our earlier studies that multiple emitting species are present for TyrA and that they are due to the ground-state rotamer populations of the phenol side chain about its C^{α}-C^{β} bond [6,7]. Consequently, we first analyzed the data in Fig. 1 by Eq. (5), trying to extract the different K_{sv} terms and fractional intensities for the three rotamers. However, the algorithm usually failed to converge on any minimum in the fitting error surface. It was obvious that we were attempting to evaluate too many variables (three K_{sv} and two of the three fractional intensities) for this type of function and data density.

To confirm that there were too many variables, Eq. (5) was used to generate synthetic data for three species with various combinations of $K_{sv}(i)$ and $f(i)$. The only way a solution could be obtained was to provide initial values (guesses) that were the same as the values used to generate the data. If the guesses were different from the known values, the algorithm failed to converge in a manner similar to that observed with real data. To see how many independent parameters could be correctly resolved from these synthetic data, we reduced the number of parameters one at a time by making that variable a constant. By this procedure, we could obtain correct K_{sv} values when all three fractional intensities were given. The ability to resolve the K_{sv} terms, however, required that the fractional intensities be nearly equivalent.

To analyze the data in Fig. 1 with Eq. (5), we first reduced the number of parameters that had to be determined by making the fractional intensities of each rotamer a constant. The fitting algorithm still did not converge; this behavior was expected based on the results of the simulation studies discussed above. Consequently, to reduce the number of unknowns further, the K_{sv} terms had to be determined independently.

The K_{sv} terms can be obtained from time-resolved fluorescence quenching studies through Eq. (9) as demonstrated in Fig. 2. The TyrA fluorescence intensity decay curves were resolved into the sum of three exponentials, with each τ_o/τ lifetime ratio a linear function of acrylamide concentration. For these experiments, a sum of three exponentials was required in the presence of acrylamide; the amplitudes were invariant with quencher concentration and close to the NMR-determined ground-state rotamer populations. Linking the populations to the amplitudes during the analysis of a fluorescence intensity decay limited the number of parameters that had to be determined [8]. This procedure reduced the variation in the lifetime values. A triple-exponential analysis was sufficient. Since the amplitudes agree with the NMR-determined rotamer populations and the lifetime ratios are linear with respect to $[Q]$, a model with three ground-state species is supported. If other processes are occurring, such as transient kinetic quenching effects [22–26], deviations in $\alpha(i)$ and $\tau_o(i)/\tau(i)$ vs $[Q]$ would have been

observed. These effects have not been detected within the resolution of these experiments.

In the absence of acrylamide, the intensity decay of TyrA can be adequately analyzed as the sum of two exponentials [6], in contrast to the triple-exponential decay that is always necessary in the presence of acrylamide. This can be explained by the difference between the value of the dynamic bimolecular quenching constant for rotamer I and that for rotamer III (Table I). Because the lifetimes of rotamers I and III in the absence of quencher are similar to each other but distinct from that of rotamer II, an analysis for two exponentials is adequate. Rotamers I and III are quenched differently, however, thus separating their lifetimes enough so that they are easily resolved. This difference in k_q values among the three rotamers demonstrates that the phenol side chain in each rotamer experiences a different environment. Since rotamers II and III have the shortest lifetimes and the largest k_q terms, it could be argued that this indicates transient kinetic effects [22–26] rather than different environments. However, if transient processes are occurring, the $k_q(i)$ should be an inverse function of $\tau_o(i)$. This is not true for this system since the largest k_q is associated with rotamer III and its intermediate lifetime. The ability to assign a k_q to a specific species further supports the rotamer model for the fluorescence intensity decay of tyrosine compounds [6,7,27]. Resolution of species-specific bimolecular quenching constants has the potential of resolving small differences in local structure as well as conformation-dependent binding interactions. Any attempt to infer the structure of TyrA based on the individual bimolecular quenching constants is premature; quenching parameters for other tyrosine compounds and quenchers are required for comparisons.

With the determination of all the dynamic quenching parameters by time-resolved fluorescence quenching, we generated a fit by Eq. (5) to the steady-state quenching data. As shown in Fig. 4, the fit generated with these dynamic parameters appears to be linear and in no way resembles the trends in the data. This lack of upward curvature is a consequence of the model. Based on simulation studies, we could not find a set of physically relevant $K_{sv}(i)$ and $f(i)$ values that results in upward curvature for Eq. (5). Usually, the expression is linear or slightly curved downward, and appreciable downward curvature occurs only if there is a large difference between K_{sv} values. Consequently, one or more additional processes aside from multiple species are implicated to cause the curvature in the steady-state data.

Static quenching mechanisms, due to their rapid depletion of the excited state before collisional processes can occur (see Theory), affect the steady-state intensity but not the lifetime. As a result, all static quenching mechanisms cause the F_o/F ratio [Eq. (1)] to increase at a rate greater than the τ_o/τ ratio. Furthermore, since a static quenching mechanism is also a function of quencher concentration, the F_o/F ratio appears to curve upward. Therefore, the data in Fig. 1 could be indicating that each rotamer is statically as well as dynamically quenched.

We were able to analyze the steady-state data in terms of two different static quenching mechanisms by using the dynamic quenching parameters as constants to reduce the number of unknowns. Thus, the largest number of parameters that had to be independently determined came from an analysis by Eq. (6) where a $V(i)$ term for each rotamer was evaluated. There were no problems in obtaining a unique solution and the fit generated by Eq. (6) was very good (Fig. 4). The V term obtained by this analysis for rotamer II was zero; an explanation of only one rotamer having kinetic but not static quenching is not immediately obvious.

The analysis of the data by Eq. (7), which accounts for each rotamer forming a ground-state complex with acrylamide, provided an equivalent fit (Fig. 5). In this model we assumed that each rotamer has the same association constant, K_a, for acrylamide binding. If the environments are different enough for each rotamer to have its own fluorescence lifetime and diffusional quenching constant, then they also might differ enough for each rotamer to have a unique K_a value. However, the ground-state interactions resulting in static quenching are expected to be weak, and any differences in the weak ground-state association constants between the rotamers would be too small to quantitate accurately. The value for the K_a obtained by this analysis, $1\,M^{-1}$, demonstrates the weak nature of this interaction. The ability of acrylamide to bind to proteins and cause static quenching has been debated, but recent results indicate that if it does bind, the binding is weak and of the order of magnitude observed here [28].

There are numerous examples in the literature of nonlinear steady-state Stern–Volmer quenching results. Often, these data are analyzed only for a single species undergoing static quenching by the model given in Eq. (3); apparently, no consideration is given to the possibility of multiple species. In addition, since experiments are often not performed to sufficiently high quencher concentrations, it is difficult to determine whether or not the Stern–Volmer plot is actually linear.

We know from the intensity decay parameters for TyrA that it is incorrect to analyze the steady-state quenching data by Eq. (3) or (4). Nevertheless, as can be seen by the residuals in Fig. 1, an acceptable fit can be obtained by Eq. (3). The evaluated parameters, re-

ported as averages of the six titrations, are $K_{sv} = 6.45\ M^{-1}$ and $V = 0.71\ M^{-1}$.

As shown above, the K_{sv} variable can be divided by the lifetime of the chromophore in the absence of quencher, τ_o, to calculate the bimolecular quenching constant, k_q. In the Stern–Volmer expression given in Eq. (2), however, it is assumed that the chromophore decays from the excited state through a kinetic mechanism yielding a single exponential. For TyrA, the fluorescence intensity decay is a sum of three exponentials. Therefore, an intensity-weighted average fluorescence lifetime in the absence of quencher, $\langle\tau_o\rangle$, must be obtained:

$$\langle\tau_o\rangle = \sum_{i=1}^{3} \alpha(i)\,\tau_o(i)^2 \Big/ \sum_{i=1}^{3} \alpha(i)\,\tau_o(i) \qquad (10)$$

Thus an average bimolecular quenching constant, $\langle k_q\rangle$, is calculated to be $3.7 \times 10^9\ M^{-1}\ s^{-1}$ based on a $\langle\tau_o\rangle$ of 1.75 ns.

If $\langle k_q\rangle$ has any significance in demonstrating the accessibility of a quencher to a system with multiple species (rotamers), it must be the same as an average bimolecular quenching constant, $\bar{k}_q$, that can be calculated from the rotamer-specific k_q terms. This average is

$$\bar{k}_q = \sum_{i=1}^{3} w(i)\,k_q(i) \qquad (11)$$

where $w(i)$ are weighting terms which must account for the relative intensity [Eq. (8)] of each rotamer as well as for its lifetime, which reflects on the amount of time available for the diffusional quenching interaction. Thus the weighting terms are expressed by

$$w(i) = \alpha(i)\,\tau_o(i)^2 \Big/ \sum_{i=1}^{3} \alpha(i)\,\tau_o(i)^2 \qquad (12)$$

When the decay parameters for the quenching of TyrA by acrylamide are used (Table I), $\bar{k}_q = 3.5 \times 10^9\ M^{-1}\ s^{-1}$, which compares very well with the value of $3.7 \times 10^9\ M^{-1}\ s^{-1}$ for $\langle k_q\rangle$.

In this instance, it appears that the K_{sv} value obtained by fitting the data to the single-species model of Eq. (3) can be used to demonstrate an average overall solvent accessability by providing an average bimolecular quenching constant. This is in spite of the fact that the curvature in the data could be adequately fit by the $e^{[Q]}$ term, which is inappropriate for the multiple-species model. [Note that the V term obtained from the analysis by Eq. (3) is about 10% of K_{sv}.] *The calculation of $\langle k_q\rangle$ required, however, that we know $\langle\tau_o\rangle$.* One can obtain a more detailed understanding of the local environment of the chromophore, however, by also performing the time-resolved quenching studies.

The steady-state data could also be represented by the multiple-species model with static quenching through the formation of a weak ground-state complex [Eq. (7)]. We therefore tried to analyze the data according to the corresponding single-species model represented by Eq. (4). The fits obtained by Eq. (4) were generally worse, and never better, than those obtained by Eq. (3). The major problem with an analysis by Eq. (4) is that the iterated parameters, K_{sv} and K_a, are indistinguishable from each other because of the symmetry of the quadratic expression [16].

In conclusion, we can resolve different k_q values for the quenching of each of the three TyrA rotamers by acrylamide. These parameters, along with the fractional intensities, have been used in a systematic approach to analyze for the presence of static quenching. By combining these two fluorescence quenching methods, we have been able to resolve and characterize the solvent accessibility of the environments of the individual rotamers of the phenol side chain about the C^{α}–C^{β} bond in TyrA. This behavior is not specific to TyrA; our preliminary results with other tyrosine-containing compounds and quenchers also indicate rotamer-specific behavior. In particular, the initial results for the quenching of TyrA by iodide ion at pH 3 indicate that the environments are influenced equally by the protonated amine since the k_q for each rotamer increases by about a factor of two.

ACKNOWLEDGMENTS

This work was supported by National Institutes of Health Grants DK-39548, DK-10080, and GM-39750 and, in part, by National Science Foundation Grant DMB-8516318. Preliminary aspects of this work were presented at the 34th Annual Meeting of the Biophysical Society, Baltimore, MD, 18–22 February 1990, and at the 10th International Biophysics Congress, Vancouver, Canada, 29 July–3 August 1990.

Our discussions with Drs. Carol A. Hasselbacher and J. B. Alexander Ross were very helpful. We also wish to thank Mr. Evan Waxman for a critical evaluation of the manuscript and for programming assistance. The comments of the reviewer were greatly appreciated.

REFERENCES

1. A. E. W. Knight and B. K. Selinger (1971) *Chem. Phys. Lett.* **10**, 43–48.

2. A. Grinvald and I. Z. Steinberg (1974) *Anal. Biochem.* **59,** 583–598.
3. D. R. James, Y. S. Liu, P. DeMayo, and W. R. Ware (1985) *Chem. Phys. Lett.* **120,** 460–465.
4. O. Stern and M. Volmer (1919) *Phys. Z.* **20,** 183–188.
5. M. R. Eftink and C. A. Ghiron (1981) *Anal. Biochem.* **114,** 199–227.
6. W. R. Laws, J. B. A. Ross, H. R. Wyssbrod, J. M. Beechem, L. Brand, and J. C. Sutherland (1986) *Biochemistry* **25,** 599–607.
7. J. B. A. Ross, W. R. Laws, A. Buku, J. C. Sutherland, and H. R. Wyssbrod (1986) *Biochemistry* **25,** 607–612.
8. J. B. A. Ross, W. R. Laws, J. C. Sutherland, A. Buku, P. G. Katsoyannis, I. L. Schwartz, and H. R. Wyssbrod (1986) *Photochem. Photobiol.* **44,** 365–370.
9. J. Paoletti and J.-B. LePecq (1969) *Anal. Biochem.* **31,** 33–41.
10. T. Azumi and S. P. McGlynn (1962) *J. Chem. Phys.* **37,** 2413–2420.
11. A. H. Kalantar (1968) *J. Chem. Phys.* **48,** 4992–4996.
12. M. Shinitzky (1972) *J. Chem. Phys.* **56,** 5979–5981.
13. C. A. Parker (1968) *Photoluminescence of Solutions,* Elsevier, New York.
14. C. A. Hasselbacher, E. Waxman, L. T. Galati, P. B. Contino, J. B. A. Ross, and W. R. Laws (1991) *J. Phys. Chem.*, in press.
15. P. R. Bevington (1969) *Data Reduction and Error Analysis for the Physical Sciences,* McGraw-Hill, New York.
16. W. R. Laws and P. B. Contino (1991) *Methods in Enzymology,* in press.
17. E. Casali, P. H. Petra, and J. B. A. Ross (1990) *Biochemistry* **29,** 9334–9343.
18. A. Weller (1961) *Prog. React. Kinet.* **1,** 187–214.
19. W. R. Laws and L. Brand (1979) *J. Phys. Chem.* **83,** 795–802.
20. D. M. Rayner, D. T. Krajcarski, and A. G. Szabo (1978) *Can. J. Chem.* **56,** 1238–1245.
21. K. J. Willis and A. G. Szabo (1991) *J. Phys. Chem.,* in press.
22. F. C. Collins and G. E. Kimball (1949) *J. Colloid Sci.* **4,** 425–437.
23. F. C. Collins (1950) *J. Colloid Sci.* **5,** 499–505.
24. T. L. Nemzek and W. R. Ware (1975) *J. Chem. Phys.* **62,** 477–489.
25. N. Joshi, M. L. Johnson, I. Gryczynski, and J. R. Lakowicz (1987) *Chem. Phys. Lett.* **135,** 200–207.
26. J. R. Lakowicz, N. B. Joshi, M. L. Johnson, H. Szmacinski, and I. Gryczynski (1987) *J. Biol. Chem.* **262,** 10907–10910.
27. P. Gauduchon and Ph. Wahl (1978) *Biophys. Chem.* **8,** 87–104.
28. M. R. Eftink and C. A. Ghiron (1987) *Biochim. Biophys. Acta* **916,** 343–349.